Applied Physics Letters

# Efficient leaky-wave antennas at terahertz frequencies generating highly directional beams

Cite as: Appl. Phys. Lett. **117**, 261103 (2020); https://doi.org/10.1063/5.0033126
Submitted: 13 October 2020 . Accepted: 16 November 2020 . Published Online: 29 December 2020

H. Guerboukha, R. Shrestha, J. Neronha, O. Ryan, M. Hornbuckle, Z. Fang, and D. M. Mittleman









AIP Publishing

Applied Physics Letters ARTICLE scitation.org/journal/apl

# Efficient leaky-wave antennas at terahertz frequencies generating highly directional beams

Cite as: Appl. Phys. Lett. **117**, 261103 (2020); doi: 10.1063/5.0033126
Submitted: 13 October 2020 · Accepted: 16 November 2020 ·
Published Online: 29 December 2020



H. Guerboukha, R. Shrestha, J. Neronha, O. Ryan, M. Hornbuckle, Z. Fang, and D. M. Mittleman[a]

## AFFILIATIONS

School of Engineering, Brown University, Providence, Rhode Island 02912, USA

[a]Author to whom correspondence should be addressed: daniel_mittleman@brown.edu

## ABSTRACT

Due to their frequency-dependent angular emission, leaky-wave antennas have been recently introduced in the terahertz band to tackle many of the challenges associated with THz wireless communications. Most previous works have exploited conventional leaky-wave waveguide architectures developed for the microwave region. In this paper, we study in detail the emission characteristics of leaky-wave antennas at THz frequencies. We show that, at these high frequencies, the wavelength-scale interaction with the aperture causes a nonuniform electric field distribution at the slot interface, which is a unique regime that is not typically encountered at lower frequencies. This effect is even more pronounced as the slot width increases to a point where the sides of the slot act as secondary leaking structures, and the well-known frequency–angle relationship is not obeyed as the energy at a given frequency is radiated in a broad range of angles. Therefore, to exploit the phase matching condition, which couples frequency to emission angle, one must use very thin rectangular slots $d \ll \lambda$, at the expense of device efficiency. To address this problem, we explore an alternate slot aperture design, in which the slot width increases linearly along its length (i.e., a trapezoidal shape). We show that this preserves the phase-matching constraint while allowing higher output coupling efficiencies. Moreover, since a wider effective aperture is used, the radiated beam is narrow in both angular directions, allowing the generation of true pencil-like THz beams.



As the demand for internet bandwidth continues its ever-growing expansion, current network systems will experience unprecedented pressure.[1] This situation has spurred research into the possibility of exploiting carrier frequencies in the terahertz band (0.1–10 THz) for wireless communications.[2–5] Communication systems at such high frequencies possess several advantages, including large bandwidths for ultra-high-speed data transmission[6–10] and highly directional beams for physically secured point-to-point links.[11–13] This directionality motivates the idea of exploiting the emission properties of leaky-wave antennas.

Leaky-wave antennas have been thoroughly studied in the microwave range[14–18] and have been recently introduced at THz frequencies. In its simplest implementation, the leaky-wave antenna is a metallic waveguide that leaks radiation through a slot cut along its length,[14] although more complex configurations exist using metamaterials, for example.[15–17,19,20] To match the phases of the propagating mode and the free-space mode, the outgoing beam emerges from the slot at a frequency-dependent angle. This one-to-one correspondence between frequency and emission angle has been used to tackle many of the challenges associated with THz communications, including frequency-division multiplexing,[21,22] link discovery,[23] beam steering,[19,20,24–27] and radar and object tracking.[28–30]

Most of these previous efforts, building on earlier work at lower frequencies, have exploited conventional leaky-wave waveguide architectures, which may not be optimized for use at THz frequencies. For example, in the microwave range, the leaking structure dimensions are always deeply subwavelength in width (e.g., a 1 mm slot width at 3 GHz ($\lambda/100$) in Ref. 17). This ensures that the guided wave is uniform across the slot width. In this limit, the radiated field pattern can be computed using a simple analytical model based on a leakage rate $\alpha$ and a sinc function [Eq. (1), below], as described in Refs. 15 and 31. In contrast, most of the recent THz implementations use a leaking structure, which is comparable to the wavelength in size [e.g., a 0.7 mm slot width at 300 GHz ($\lambda/1.42$) in Ref. 22]. In this regime, the interaction of the wave with the leaking structure at the wavelength scale can no longer be neglected. This effect is even more pronounced as the slot width increases, to a point where the beam is radiated in a broad range of angles, in sharp contrast to the predictions of Eq. (1); the output no longer obeys the simple frequency–angle relationship predicted by the wave vector matching constraint.

To produce an output beam that respects the frequency–angle relation, one is limited to use very thin rectangular slots. Clearly, this comes at the expense of device efficiency as the radiated energy (per

slot length) is then very low. This is a significant drawback since power generation at THz frequencies is still an important challenge.[32–34] Here, we address this problem by introducing an alternate slot geometry, where the slot width increases linearly along its length (i.e., a trapezoidal shape). We show that this design permits higher output coupling efficiencies while preserving the phase-matching relation. Also, since the trapezoidal slot has a wider effective aperture, the radiated beam is narrow in both angular directions, which is not the case for a conventional rectangular slot aperture.

We consider a parallel plate waveguide [Fig. 1(a)] excited in the fundamental transverse electric ($TE_1$) mode.[35,36] Assuming that the electric field is polarized in the $x$ direction and the slot is oriented along the z axis (the propagation direction for the guided wave), the far-field radiation pattern emitted from a narrow slot is given by:

$$E_x^{\mathrm{rad}}(\theta) \propto \int_{-L/2}^{L/2} e^{-j\beta_z z} e^{-\alpha z} e^{jk_0 \sin(\theta) z} dz = L\,\mathrm{sinc}\left[(\beta_z - k_0 \sin\theta - j\alpha)\frac{L}{2}\right], \quad (1)$$

where $\theta$ is the elevation angle defined in Fig. 1(a) (assuming $\phi = 0$), $L$ is the slot length, $k_0 = \omega/c$ is the free-space wavenumber, $\alpha$ is the leakage rate for radiation coupling from the waveguide into free space through the slot, and $\mathrm{sinc}(x) = \sin(x)/x$. For the fundamental $TE_1$ mode of a parallel plate waveguide with an air core, the propagation constant is $\beta_z = \sqrt{k_0^2 - (\pi/h)^2}$, where $h$ is the plate separation.

From Eq. (1), one can see that the output radiation peaks at the angle defined by the phase-matching condition $\beta_z = k_0 \cos\theta$, which leads to the well-known relation:

$$\nu(\theta) = \frac{c}{2h \sin\theta}. \quad (2)$$

Equations (1) and (2) are valid for leaky-wave antennas featuring slots of widths smaller than the wavelength. This is because Eq. (1) is essentially a diffraction integral over the length of the slot aperture; the integral over the width is ignored because the electric field distribution is assumed to be uniform in that direction. If the slot width becomes comparable to or larger than the wavelength, then this assumption may no longer be valid. To explore this, we perform numerical simulations using the finite element method (FEM) by exciting the input of the waveguide with a $TE_1$ mode. The electromagnetic fields on the slot, obtained from the FEM simulations, are then used to calculate the far-field radiation pattern using a refined version of Eq. (1), the Stratton–Chu diffraction integral.[37,38]

Figures 1(b)–1(d) show the results for a leaky-wave antenna excited at 200 GHz, a frequency that lies in the single-mode operation band (150–300 GHz) of a parallel plate waveguide with $h = 1$ mm. The rectangular slot has a width $w = 0.25$ mm and a length $L = 20$ mm. Figure 1(b) shows the $x$-polarized electric field on the slot. For such a narrow slot, the electric field is uniform across the width of the slot, while showing a behavior compatible with the integrand of Eq. (1), namely, a sine wave with an exponentially decaying amplitude. This is further confirmed by Fig. 1(c) [cross section in the center of Fig. 1(b)], where such a function is well fitted to the numerical result. The far-field radiation pattern [Fig. 1(d)] agrees to the prediction of the conventional diffraction integral [Eq. (1)] in the form of the sinc function. This ensures that the phase-matching condition is respected over the single-mode operation band [Fig. 1(e)], resulting in a good agreement between the radiated electric field and Eq. (2) [shown as a dashed line in Fig. 1(e)].

The analytical expression Eq. (1) is valid when the wavelength $\lambda$ is larger than the slot width. For example, for the results shown in Figs. 1(b)–1(d), the width is a sixth of the wavelength. However, such small widths also restrict the amount of energy leaking out of the slot. A naive solution to this problem would be to increase the slot width. However, this approach has its limits; when the slot width becomes too large, the device stops behaving as a conventional leaky-wave antenna. Figure 2(a) shows the electric field distributions directly underneath the slot at 200 GHz for slot widths $w = \{1, 5, 10, 20\}$ mm.

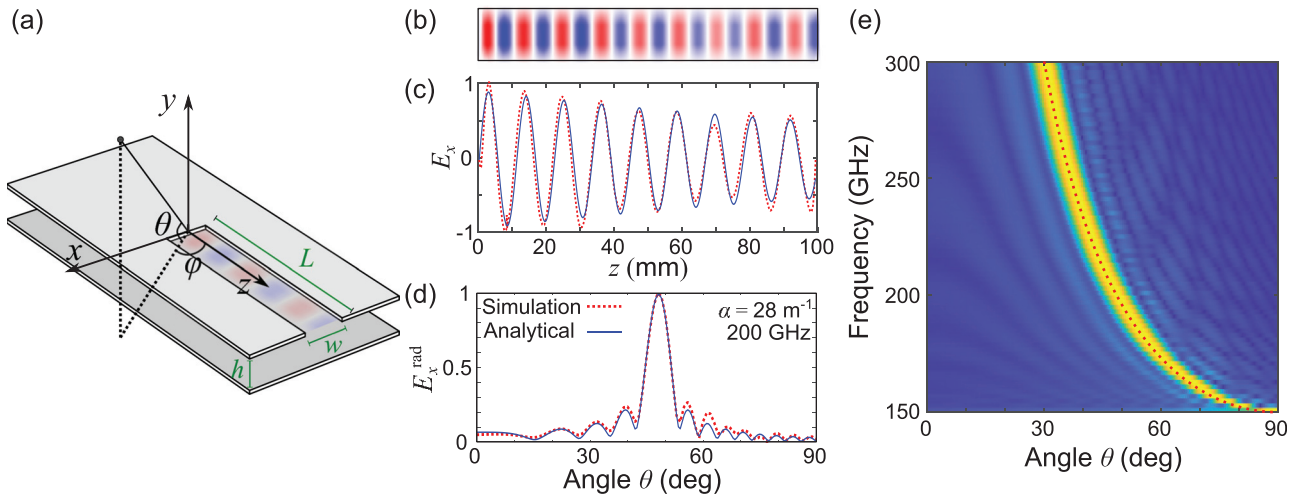


**FIG. 1.** (a) Leaky-wave antenna geometry. (b)–(e) Numerical simulations for a 0.25 mm slot width (200 GHz). (b) Electric field on the slot and (c) cross section (red dotted curve). Blue line: analytic function $\sin(\beta_z z)e^{-\alpha z}$. (d) Far-field radiation pattern (electric field, $\phi = 0$) calculated with the Stratton–Chu integral (red dotted line) and fitted with Eq. (1), $\alpha = 28\,\mathrm{m}^{-1}$ (blue line). (e) Far-field radiation pattern in the single-mode operation band. Red dashed line: frequency–angle relation [Eq. (2)].

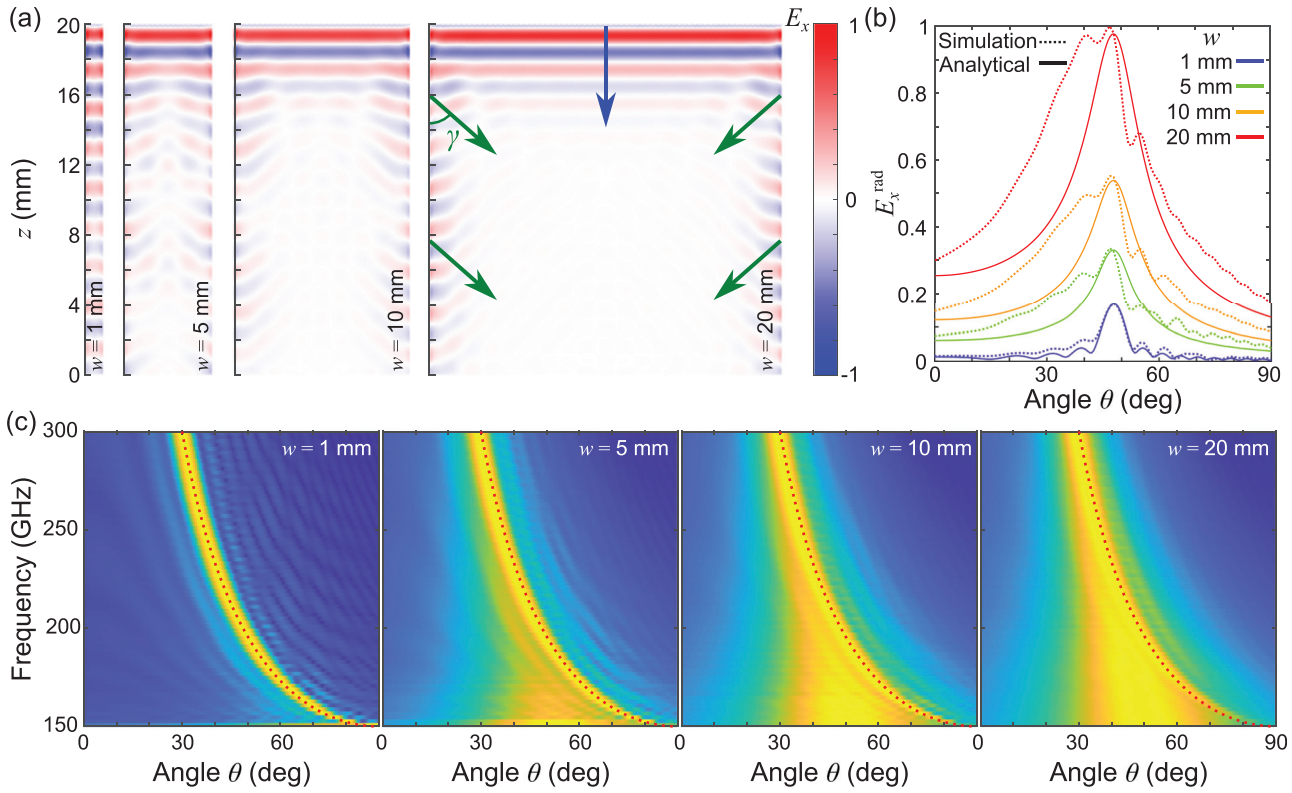


**FIG. 2.** (a) Electric field (200 GHz) for rectangular slots of varying widths (b) and far-field radiation pattern (electric field, $\phi = 0$) calculated with the Stratton–Chu integral (dotted lines) and tentatively fitted with Eq. (1) (bold lines). (c) Far-field radiation in the single-mode operation band. Red dashed line: frequency–angle relation [Eq. (2)].

In these simulations, we assume that the width of the waveguide is infinite and that the input $TE_1$ mode extends infinitely in the $\pm x$ directions, allowing us to disregard the effect of finite beam size and the edges of the waveguide. As the slot width increases, the electric field is no longer a simple sine wave with a decaying amplitude but is a complicated combination of the $TE_1$ mode leaking from the front and the sides of the slot. Then, the guided wave is no longer uniform across the slot width and the linear integral used in Eq. (1) must be replaced by the 2D Stratton–Chu diffraction integral over the slot surface. Hence, the analytical expression (the sinc function) fails to accurately describe the far-field radiation pattern. This is confirmed by Fig. 2(b), where the far-field patterns obtained with the 2D Stratton–Chu integral (dotted lines) are tentatively fitted to the sinc function using a least squares fitting procedure in which $\alpha$ is the freely variable fit parameter (bold lines). The results confirm that Eq. (1) is a good approximation for the 1 mm slot but increasingly fails to capture the far-field behavior as the slot becomes wider. Another major drawback of wide slots can be seen in Fig. 2(c), where the phase-matching relation is no longer respected, and the radiated electric field at a single frequency becomes broad in the $\theta$ direction. These are major disadvantages in many of the envisioned applications of these devices for THz systems; having a narrow beam emitted with a frequency-dependent direction is one of the main attractions of leaky-wave antennas at THz frequencies.

From Fig. 2(a), we observe that radiation leaking from the front (blue arrows) and the sides (green arrows) of the slot contributes to the electric field directly under the slot and, therefore, to the far-field radiation pattern. The front leaking propagates along the $z$ axis with a propagation vector in the same direction as the original $TE_1$ mode's wave vector. Therefore, the far-field radiation pattern from this component adheres to the phase-matching constraint [Eq. (2)] in the $yz$ plane ($\phi = 0$). In contrast, the radiation leaking from the sides is evanescent and emerges with an angle $\gamma$ relative to the side of the slot interface. This leads to a nonuniform electric field distribution across the slot. In fact, it is possible to treat the two sides of the slot as a pair of secondary leaking structures with their own phase-matching condition, although in the $xz$ plane ($\theta = 0$) rather than the $yz$ plane. This is confirmed numerically by Fig. 3(a), where we show that the side leaking output angle $\gamma$ evolves with frequency following the same phase-matching relation of Eq. (2) but in the $xz$ plane. One consequence is that, at higher frequencies, the side leaking radiation emerges closer to the $z$ axis, explaining why the far-field radiation pattern computed in Fig. 2(c) tends to more closely follow the original phase-matching condition there.

With this understanding, we can now design an alternate slot aperture that minimizes the impact of radiation leaking from the slot sides. We introduce a trapezoidal slot aperture, with a linear increase in the slot width along its length (from $w_1$ to $w_2$). Figure 3(b) shows the electric field for various trapezoids with $w_1 = 1$ mm and varying output dimensions $w_2 = \{5, 10, 20\}$ mm. Figure 3(b) (trapezoids) can be compared with Fig. 2(a) (rectangles). For the rectangular slots, the

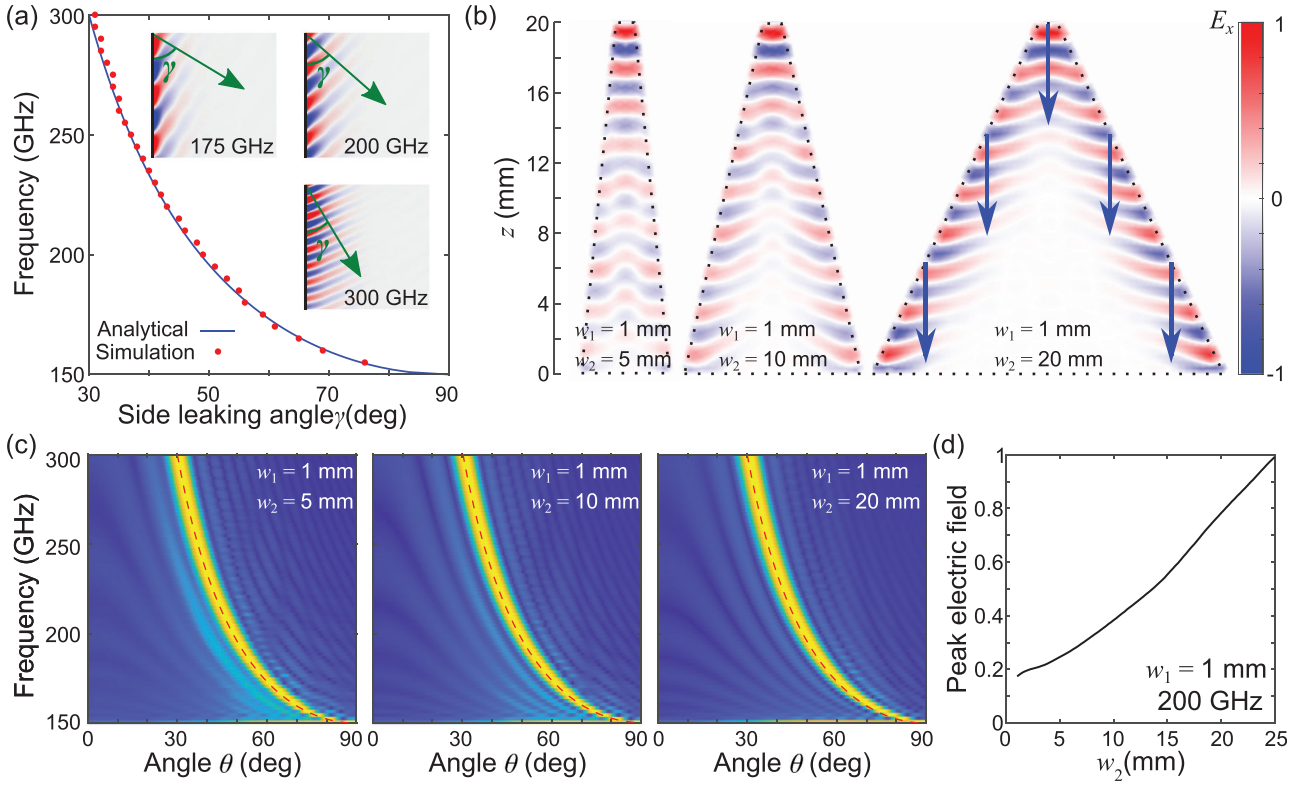


**FIG. 3.** (a) Side leaking angle $\gamma$, simulation (red dots), and frequency–angle relation (blue line). Inset: electric field leaking from the slot side at different frequencies. (b) Electric field (200 GHz) for trapezoidal slots of varying $w_2$, (c) far-field radiation (electric field, $\phi = 0$) in the single-mode operation band. Red dashed line: frequency/angle relation [Eq. (2)]. (d) Normalized amplitude of the radiated peak electric field as a function of $w_2$.

electric field is largest (in amplitude) at the front end of the rectangular slot since the side leaking relies on inefficient evanescent coupling. In contrast, the slot boundary in the trapezoidal slot has a dominant component perpendicular to the $z$ axis. This leads to efficient coupling along the entire slot length and outgoing radiation arising from waves that mostly propagate along the $z$ axis (mainly with a $\beta_z$ component). As a result, the phase-matching condition is respected in the desired direction (i.e., in the $yz$ plane, $\phi = 0°$) even when increasing the value of $w_2$. We confirm this prediction by computing the corresponding radiation patterns throughout the single-mode operation band [Fig. 3(c), which can be compared to Fig. 2(c)]. Another significant advantage is that the peak amplitude of the radiated electric field increases with $w_2$. This is a consequence of the fact that more energy is permitted to leak out of the waveguide, leading to a larger peak field in the far-field radiation pattern [Fig. 3(e)]. For example, our results show that a trapezoidal slot with $w_2 = 20$ mm (that we demonstrate experimentally below) radiates about 20 times more power than a rectangle of 1 mm width.

We verify these conclusions with experimental measurements by fabricating several leaky-wave waveguides using the hot stamping technique.[39,40] We excite the $TE_1$ mode with a frequency multiplier source at 200 GHz and measure, in the far field, the power emitted from the slot using a calibrated Schottky diode[41] [Fig. 4(a)]. Figure 4(b) shows the power as a function of the angle for a rectangular (blue line, $w = 20$ mm) and a trapezoidal slot (red line, $w_1 = 1$ mm, $w_2 = 20$ mm). As expected, the trapezoidal slot is more directional and has a maximum at the angle predicted with Eq. (2), whereas the rectangular slot emits in a broad range of angles. The dashed lines correspond to the results obtained with the numerical simulations using the same geometrical parameters and with a Gaussian $TE_1$ mode where the width was experimentally measured using a knife-edge technique. Both simulation results (rectangle and trapezoid) were normalized to the peak power of the experimental result of the rectangular aperture. The excellent agreement with the experiment highlights the usefulness of our numerical approach to predict far-field patterns but also the importance of measuring the input conditions to reproduce the experiment. We note that both apertures show comparable performance in terms of peak power, even if the trapezoid aperture has about half or the rectangular aperture area. For the trapezoid, one can change the peak power by varying the output width $w_2$, Fig. 4(c), confirming this anticipated increase in efficiency. Using a broadband time-domain spectrometer, we measure the output spectrum as a function of the far-field angle [Fig. 4(d)]. Again, as predicted by the FEM simulations, the trapezoidal slot produces a far-field pattern, which agrees much more closely with the conventional phase-matching relation [Eq. (2)] than does the rectangular slot.

Finally, we consider the characteristics of the far-field radiation pattern in the azimuthal angle $\phi$. From the point of view of diffraction

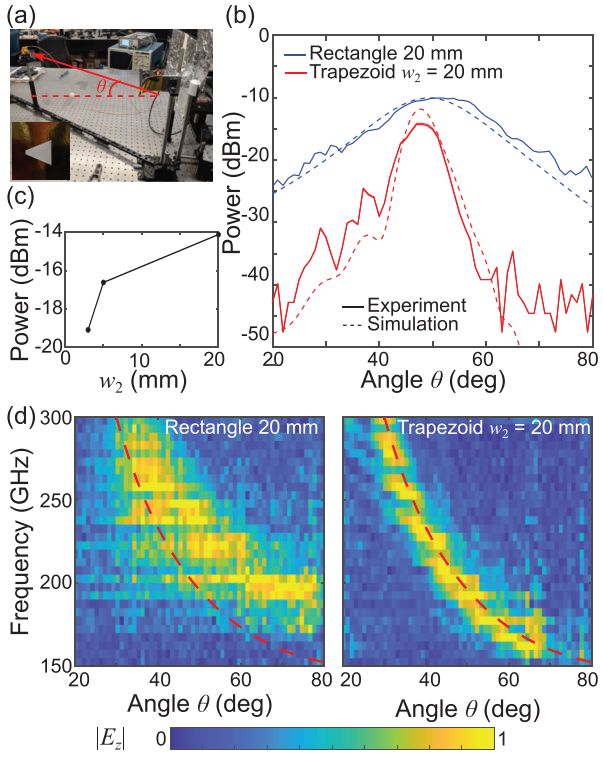


**FIG. 4.** (a) Experimental setup. Inset: fabricated trapezoidal aperture. (b) Power (200 GHz) as a function of the elevation angle $\theta$ for a rectangular slot of 20 mm (blue line) and a trapezoidal slot with $w_1 = 1$ mm and $w_2 = 20$ mm (red line), measurement (bold line) and simulation (dashed line). (c) Measured peak power for various trapezoids ($w_1 = 1$ mm). (d) Spectrum (electric field) for the rectangular slot of 20 mm and the trapezoid with $w_2 = 20$ mm.

theory, waves emitted from a large aperture produce a narrow beam, while those emitted from a narrow aperture generate a wide beam. In our case, the slot length $L$ is responsible for the beam width in the direction of the elevation angle $\theta$. This can be verified analytically by looking at the influence of $L$ in the sinc function [Eq. (1)]. Similarly, the beam width in the azimuthal direction $\phi$ depends on the slot width. Figures 5(a)–5(c) show the radiated electric field and directivities, computed using FEM simulations, for rectangular slots of 1 and 20 mm, as well as a trapezoid with $w_1 = 1$ mm and $w_2 = 20$ mm. The slot of small width produces a wide fan-shaped beam in the azimuthal angle $\phi$ [Fig. 5(a)], while it is the opposite for the large width slot [Fig. 5(b)]. For the trapezoidal shape [Fig. 5(c)], since the radiated field has contributions from the front and the sides of the slot, the radiated beam width can be controlled by changing $L$ (for the $\theta$ direction) and $w_2$ (for the $\phi$ direction). By increasing $w_2$, one can decrease the beam width in the $\phi$ direction, thus leading to a much narrower beam than could be obtained with any rectangular shape, in both angular directions. Figure 5(d) shows the predicted evolution of the beam width as a function of $w_2$, demonstrating the possibility of obtaining a true pencil-like beam from a trapezoidal slot. We further demonstrate this experimentally using our frequency multiplier setup at 200 GHz. We measure the radiated power as a function of the azimuthal angle $\phi$ [for $\theta = 48°$, the angle predicted from Eq. (2)] for various slot designs

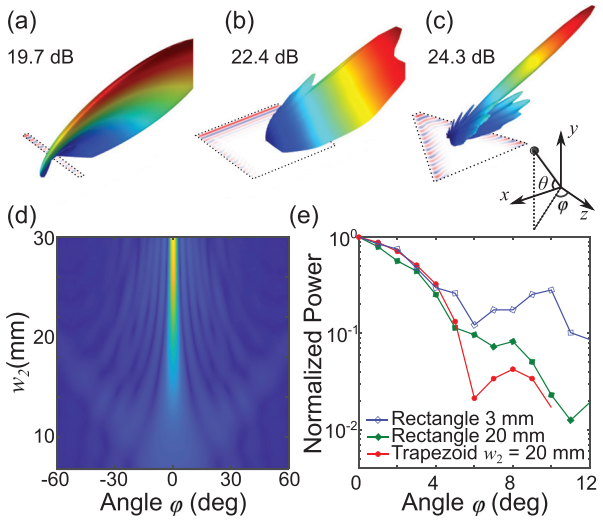


**FIG. 5.** (a) Radiated power for 1 mm, (b) 20 mm rectangular slot, (c) and trapezoid with $w_1 = 1$ mm, $w_2 = 20$ mm. The directivities are indicated. (d) Far-field pattern (electric field, $\theta = 48°$) as a function of the azimuthal angle $\phi$. (e) Normalized measured power for rectangular slots of 3 mm (blue line) and 20 mm (green line), and a trapezoidal slot with $w_1 = 1$ mm and $w_2 = 20$ mm.

[Fig. 5(e)]. As expected, the rectangular slot of 3 mm (blue line) showed the largest beam width, while it was narrower for both the rectangular slot of 20 mm and the trapezoid with $w_1 = 1$ mm and $w_2 = 20$ mm. The ability to generate a beam with low angular divergence in both $\theta$ and $\phi$ will be valuable in THz wireless networks, serving multiple clients with non-interfering spatially multiplexed beams.[21–23]

In conclusion, we studied the far-field radiation of the leaky-wave antenna at THz frequencies. We found that, when the slot width is comparable to or larger than the wavelength, the electric field directly under the slot is nonuniform, which means that the conventional analytical description of the far-field radiation pattern is less applicable. This effect is even more pronounced as the slot width increases, to a point where the sides of the slot can act as independent leaking structures. Then, the output beam is radiated in a broad range of angles, and the usual phase-matching relationship can no longer be observed. Therefore, to produce an output beam that rigorously respects the frequency/angle relation, very thin rectangular slots must be used, at the expense of device efficiency. To address this problem, we propose a trapezoidal slot geometry where the width linearly increases along its length. By doing so, we can preserve the desirable one-to-one relation between frequency and angle while enabling higher output coupling efficiencies. Moreover, since a wider effective aperture is used, the radiated beam is narrow in both angular directions. These results should improve the performance of leaky-wave antennas, which have a wide range of possible uses in future terahertz systems.

## AUTHORS' CONTRIBUTIONS

H.G. and R.S. contributed equally to this work.

This work was supported by the U.S. National Science Foundation. H. Guerboukha acknowledges the support from Fonds de recherche du Québec—Nature et Technologies (FRQNT).

## DATA AVAILABILITY

The data that support the findings of this study are available from the corresponding author upon reasonable request.

## REFERENCES


[1]Cisco, https://www.cisco.com/c/en/us/solutions/collateral/executive-perspectives/annual-internet-report/white-paper-c11-741490.html for "Cisco Annual Internet Report (2018–2023) White Paper (March 2020 Update)," 2020.

[2]T. Nagatsuma, S. Horiguchi, Y. Minamikata, Y. Yoshimizu, S. Hisatake, S. Kuwano, N. Yoshimoto, J. Terada, and H. Takahashi, "Terahertz wireless communications based on photonics technologies," Opt. Express **21**, 23736 (2013).

[3]T. Nagatsuma, G. Ducournau, and C. C. Renaud, "Advances in terahertz communications accelerated by photonics," Nat. Photonics **10**, 371–379 (2016).

[4]D. M. Mittleman, "Perspective: Terahertz science and technology," J. Appl. Phys. **122**, 230901 (2017).

[5]K. Sengupta, T. Nagatsuma, and D. M. Mittleman, "Terahertz integrated electronic and hybrid electronic–photonic systems," Nat. Electron. **1**, 622–635 (2018).

[6]H.-J. Song, K. Ajito, Y. Muramoto, A. Wakatsuki, T. Nagatsuma, and N. Kukutsu, "24 Gbit/s data transmission in 300 GHz band for future terahertz communications," Electron. Lett. **48**, 953 (2012).

[7]H.-J. Song, J.-Y. Kim, K. Ajito, N. Kukutsu, and M. Yaita, "50-Gb/s direct conversion QPSK modulator and demodulator MMICs for terahertz communications at 300 GHz," IEEE Trans. Microwave Theory Tech. **62**, 600–609 (2014).

[8]S. Koenig, D. Lopez-Diaz, J. Antes, F. Boes, R. Henneberger, A. Leuther, A. Tessmann, R. Schmogrow, D. Hillerkuss, R. Palmer, T. Zwick, C. Koos, W. Freude, O. Ambacher, J. Leuthold, and I. Kallfass, "Wireless sub-THz communication system with high data rate," Nat. Photonics **7**, 977–981 (2013).

[9]K. Nallappan, H. Guerboukha, C. Nerguizian, and M. Skorobogatiy, "Live streaming of uncompressed HD and 4K videos using terahertz wireless links," IEEE Access **6**, 58030–58042 (2018).

[10]T. Harter, C. Füllner, J. N. Kemal, S. Ummethala, J. L. Steinmann, M. Brosi, J. L. Hesler, E. Bründermann, A. S. Müller, W. Freude, S. Randel, and C. Koos, "Generalized Kramers–Kronig receiver for coherent terahertz communications," Nat. Photonics **14**, 601 (2020).

[11]J. Ma, R. Shrestha, J. Adelberg, C.-Y. Yeh, Z. Hossain, E. Knightly, J. M. Jornet, and D. M. Mittleman, "Security and eavesdropping in terahertz wireless links," Nature **563**, 89–93 (2018).

[12]V. Petrov, D. Moltchanov, J. M. Jornet, and Y. Koucheryavy, "Exploiting multipath terahertz communications for physical layer security in beyond 5G networks," in *IEEE INFOCOM 2019—IEEE Conference on Computer Communications Workshops (INFOCOM WKSHPS)* (IEEE, 2019), pp. 865–872.

[13]C.-Y. Yeh, Y. Ghasempour, Y. Amarasinghe, D. M. Mittleman, and E. W. Knightly, "Security in terahertz WLANs with leaky wave antennas," in *Proceedings of the 13th ACM Conference on Security and Privacy in Wireless and Mobile Networks* (ACM, 2020), pp. 317–327.

[14]L. Goldstone and A. Oliner, "Leaky-wave antennas I: Rectangular waveguides," IRE Trans. Antennas Propag. **7**, 307–319 (1959).

[15]A. Oliner and D. R. Jackson, "Leaky-wave antennas," in *Antenna Engineering Handbook* (McGraw Hill, 2007), p. 12.

[16]D. R. Jackson, C. Caloz, and T. Itoh, "Leaky-wave antennas," Proc. IEEE **100**, 2194–2206 (2012).

[17]L. Liu, C. Caloz, and T. Itoh, "Dominant mode leaky-wave antenna with backfire-to-endfire scanning capability," Electron. Lett. **38**, 1414–1416 (2002).

[18]S. Taravati and C. Caloz, "Mixer-duplexer-antenna leaky-wave system based on periodic space-time modulation," IEEE Trans. Antennas Propag. **65**, 442–452 (2017).

[19]W. Fuscaldo, S. Tofani, D. C. Zografopoulos, P. Baccarelli, P. Burghignoli, R. Beccherelli, and A. Galli, "Systematic design of THz leaky-wave antennas based on homogenized metasurfaces," IEEE Trans. Antennas Propag. **66**, 1169–1178 (2018).

[20]W. Fuscaldo, P. Burghignoli, P. Baccarelli, and A. Galli, "A reconfigurable substrate-superstrate graphene-based leaky-wave THz antenna," IEEE Antennas Wireless Propag. Lett. **15**, 1545–1548 (2016).

[21]N. J. Karl, R. W. McKinney, Y. Monnai, R. Mendis, and D. M. Mittleman, "Frequency-division multiplexing in the terahertz range using a leaky-wave antenna," Nat. Photonics **9**, 717–720 (2015).

[22]J. Ma, N. J. Karl, S. Bretin, G. Ducournau, and D. M. Mittleman, "Frequency-division multiplexer and demultiplexer for terahertz wireless links," Nat. Commun. **8**, 729 (2017).

[23]Y. Ghasempour, R. Shrestha, A. Charous, E. Knightly, and D. M. Mittleman, "Single-shot link discovery for terahertz wireless networks," Nat. Commun. **11**, 2017 (2020).

[24]M. Esquius-Morote, J. S. Gomez-Diaz, and J. Perruisseau-Carrier, "Sinusoidally modulated graphene leaky-wave antenna for electronic beamscanning at THz," IEEE Trans. Terahertz Sci. Technol. **4**, 116–122 (2014).

[25]X. C. Wang, W. S. Zhao, J. Hu, and W. Y. Yin, "Reconfigurable terahertz leaky-wave antenna using graphene-based high-impedance surface," IEEE Trans. Nanotechnol. **14**, 62–69 (2015).

[26]A. A. Tavallaee, B. S. Williams, P. W. C. Hon, T. Itoh, and Q. S. Chen, "Terahertz quantum-cascade laser with active leaky-wave antenna," Appl. Phys. Lett. **99**, 141115 (2011).

[27]D. Dancila, B. Beuerle, U. Shah, J. Oberhammer, and A. Rydberg, "Leaky wave antenna at 300 GHz in silicon micromachined waveguide technology," in *2019 44th International Conference on Infrared, Millimeter, and Terahertz Waves (IRMMW-THz)* (IEEE, 2019), pp. 1–2.

[28]K. Murano, I. Watanabe, A. Kasamatsu, S. Suzuki, M. Asada, W. Withayachumnankul, T. Tanaka, and Y. Monnai, "Low-profile terahertz radar based on broadband leaky-wave beam steering," IEEE Trans. Terahertz Sci. Technol. **7**, 60–69 (2017).

[29]H. Matsumoto, I. Watanabe, A. Kasamatsu, and Y. Monnai, "Integrated terahertz radar based on leaky-wave coherence tomography," Nat. Electron. **3**, 122–129 (2020).

[30]Y. Amarasinghe, R. Mendis, and D. M. Mittleman, "Real-time object tracking using a leaky THz waveguide," Opt. Express **28**, 17997 (2020).

[31]A. Sutinjo, M. Okoniewski, and R. H. Johnston, "Radiation from fast and slow traveling waves," IEEE Antennas Propag. Mag. **50**, 175–181 (2008).

[32]D. M. Mittleman, "Frontiers in terahertz sources and plasmonics," Nat. Photonics **7**, 666–669 (2013).

[33]R. A. Lewis, "A review of terahertz sources," J. Phys. D **47**, 374001 (2014).

[34]H. Guerboukha, K. Nallappan, and M. Skorobogatiy, "Toward real-time terahertz imaging," Adv. Opt. Photonics **10**, 843 (2018).

[35]R. Mendis and D. M. Mittleman, "An investigation of the lowest-order transverse-electric (TE_1) mode of the parallel-plate waveguide for THz pulse propagation," J. Opt. Soc. Am. B **26**, A6 (2009).

[36]R. Mendis and D. M. Mittleman, "Comparison of the lowest-order transverse-electric (TE_1) and transverse-magnetic (TEM) modes of the parallel-plate waveguide for terahertz pulse applications," Opt. Express **17**, 14839 (2009).

[37]J. A. Stratton and L. J. Chu, "Diffraction theory of electromagnetic waves," Phys. Rev. **56**, 99–107 (1939).

[38]J. A. Stratton, "Radiation," in *Electromagnetic Theory* (John Wiley & Sons, Inc., 2015), pp. 424–481.

[39]H. Guerboukha, Y. Cao, K. Nallappan, and M. Skorobogatiy, "Super-resolution orthogonal deterministic imaging technique for terahertz subwavelength microscopy," ACS Photonics **7**, 1866–1875 (2020).

[40]Y. Cao, K. Nallappan, H. Guerboukha, G. Xu, and M. Skorobogatiy, "Additive manufacturing of highly reconfigurable plasmonic circuits for terahertz communications," Optica **7**, 1112 (2020).

[41]J. Ma, R. Shrestha, L. Moeller, and D. M. Mittleman, "Invited article: Channel performance for indoor and outdoor terahertz wireless links," APL Photonics **3**, 051601 (2018).